THE JOURNAL OF PHYSICAL CHEMISTRY C

ARTICLE

pubs.acs.org/JPCC

Band Engineering in Graphene with Superlattices of Substitutional Defects

S. Casolo,*[,†] R. Martinazzo,*[,†,‡] and G. F. Tantardini[†,‡]

[†]Dipartimento di Chimica Fisica ed Elettrochimica, Università degli Studi di Milano, via Golgi 19, 20133 Milan, Italy

[‡]CIMaINa, Interdisciplinary Center for Nanostructured Materials and Interfaces, via Celoria 16, 20133 Milan, Italy

Supporting Information

ABSTRACT: We investigate graphene superlattices of nitrogen and boron substitutional defects. Using symmetry arguments and electronic structure calculations we show how such superlattices can be used to modify graphene band structure. Specifically, depending on the superlattice symmetry, the structures considered here can either preserve the Dirac cones (D_{6h} superlattices) or open a band gap (D_{3h}). Relevant band parameters (carrier effective masses, group velocities, and gaps, when present) are found to depend on the superlattice constant n as $1/n^p$ where p is in the range 1−2, depending on the case considered. Overall, the results presented here show how one can tune the graphene band structure to a great extent by modifying a few superlattice parameters.

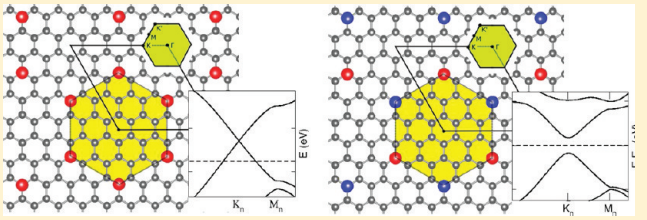

INTRODUCTION

Single-layer graphene is a very promising material for future silicon-free nanoelectronics. The peculiar character of its charge carriers comes from the intersection of the π/π^* electronic bands occurring at the corners of its hexagonal Brillouin zone. This gives rise to the so-called Dirac cones at the Fermi level and makes graphene a zero-gap semiconductor[1] in which low-energy excitations behave as massless, chiral Dirac particles.[2,3] In turn, this implies a series of interesting physical effects that open new perspectives for fabricating novel electronic devices,[4] e.g., high-performance transistors for radiofrequency applications.[5,6] In this perspective, the possibility of engineering graphene's band structure by introducing defects, strains, or external potentials has gained importance in the recent past, in particular for opening a gap in the band structure which is essential to design logic devices. Indeed, the nonvanishing residual conductance of intrinsic graphene avoids the complete current pinch-off in the pristine material,[7,8] thereby limiting the on−off ratio to $\sim 10^1$−10^2. A number of controlled techniques for energy band engineering have been proposed other than the actively pursued goal to obtain nanoribbons of controlled size and edge geometry. Most of them are based on the use of superlattices of external potentials[9,10] or defects such as holes[11,12] and adsorbates.[13] Controlled vacancies on graphene,[14] as well as large holes symmetrically arranged to form graphene antidots,[15] have actually been realized with modern lithographic and self-assembling techniques. Preferential sticking of atoms induced by Moiré patterns[16] or by other electronic effects[17,18] could also induce a superlattice ordering that modifies graphene energy bands. Likewise, there is a great hope that novel bottom-up techniques[19] may be applied to fabricate atomically precise graphenic structures as already shown for nanoribbons.[20] These approaches might allow us to realize in the near future graphene-related two-dimensional materials with *modified* characteristics, e.g., linearly dispersing bands with variable Fermi velocities or semiconducting structures. In this paper, we focus on atomically precise superlattices of substitutional atoms. The present work connects to and extends a recent work[21] where we have shown that in properly designed superlattices of holes or adatoms one can open a gap *without* breaking graphene point symmetry, i.e., preserving the pseudorelativistic behavior of charge carriers which makes graphene so attractive. The structures suggested in ref 21 have π vacancies (hence missing p_z orbitals) at the sites of a honeycomb superlattice, as a consequence of the introduction of C vacancies (holes) or chemisorption of simple atomic species. Here we consider similar, highly symmetric structures but with π vacancies replaced by boron and nitrogen. Similar defects have been recently considered for tuning the electronic properties of graphene nanoribbons and other carbon-based structures suggesting that, when arranged to form particular structures, they can turn the material into a semiconductor or a half-metal.[22−24] Half-metallicity and the other many-body effects in such structures open new perspectives in the field of carbon-based materials for spintronic applications: for a recent review, see refs 25 and 26 and references therein.

In this paper, we show that, depending on the superlattice symmetry, one can obtain either electron (hole) doped substrates with pseudorelativistic massless carriers or semiconducting structures

Received: October 11, 2010
Revised: December 17, 2010
Published: February 09, 2011

Table 1. Parameters Used in the Tight-Binding Hamiltonian[a]

atom	ε	t_1	t_2	t_3
C	0.000	−2.900	+0.175	−0.155
B	−1.5225	+1.450	-	-
N	+1.5225	−1.450	-	-

[a] All the values are in eV.

with a quasi-conical dispersion, and with the help of electronic structure calculations (tight-binding and density functional theory), we determine carrier velocities, effective masses, and band gaps (when present) as functions of the superlattice periodicity. The focus is on boron and nitrogen, mainly because of the fast progresses in methods for the controlled synthesis of B and N doped graphenes. For instance, Panchakarla et al.[27] have recently shown how it is possible to insert B or N dopants in graphene by adding the correct precursors in the arc discharge chamber, while Ci et al.[28] have reported the synthesis of large islands of boron nitride embedded in graphene by atomic layer deposition techniques. Methods to selectively replace C atoms in the graphene lattice have also been proposed,[29] thereby suggesting that the superlattice structures considered in this paper might soon become feasible.

The paper is organized as follows. In the next section we summarize the computational details of the calculations. Then, we show how *p*- (*n*-) doped graphene-like structures result when substitutional defects are arranged in *honeycomb* superlattices, whereas semiconducting structures with quasi-conical dispersion (massive Dirac carriers) result either from a *hexagonal* superlattice or from a honeycomb codoped superlattice. Finally, we summarize and conclude.

Throughout this paper we define the superlattice periodicity using Wood's notation, i.e., by multiplying graphene's two-dimensional lattice vectors by the integer (superlattice) constant *n*.

COMPUTATIONAL METHODS

The results shown in the next sections have been obtained from both tight-binding (TB) and density functional theory (DFT) electronic structure calculations. In the first case we diagonalized the usual tight-binding Hamiltonian for graphene $\pi-\pi^*$ system, applying periodic boundary conditions and including hopping terms up to the third nearest neighbors. The on-site energies ε_i and hopping terms t_1, t_2, and t_3 (for nearest, next-to-nearest, and next-to-next-nearest neighbors, respectively) are those proposed by Nanda et al.[30] They were fitted to accurate all-electron calculations to correctly reproduce the Fermi velocity of single-layer graphene. For the dopant atoms, we only considered hoppings to nearest-neighbor sites. Their values (t_1), as well as those of the on-site energies (ε_i), are those introduced by Peres et al.,[31] who have already successfully used them to study electronic effects in doped graphene. A summary of the TB parameters is listed in Table 1.

First-principles DFT calculations were performed with the help of the VASP suite,[32,33] using a supercell approach. Core electrons were taken into account by projector augmented wave (PAW) pseudopotentials, while for valence a 500 eV plane wave cutoff was used. To correctly represent the defect-induced charge inhomogeneities, we used the Perdew−Burke−Ernzerhof (PBE) gradient-dependent exchange and correlation functional.[34] Band structures were sampled by a Γ centered *k*-points grid, never sparser than $6 \times 6 \times 1$ to include every special point in the Brillouin zone (BZ).

The TB parametrization was tested by comparing the band structure of a few superlattices along the Γ−K−M−K′−Γ path with accurate DFT results. In every case, the adopted parametrization was found to be accurate enough to reproduce the bands close to the Fermi energy.

Therefore, we computed DFT band structures for $n \times n$ graphene superlattices up to $n = 14$, and for larger structures we relied on TB calculations only.

RESULTS AND DISCUSSION

Graphene's peculiar electronic structure is strictly related to the point symmetry of its lattice, D_{6h} in the Shönflies notation. In the Brillouin zone, for each Bloch electronic state with *k* vector **k**, the relevant symmetry elements are those which either leave **k** invariant or transform it into one of its equivalent images, i.e., $\mathbf{k} \rightarrow \mathbf{k} + \mathbf{G}$, **G** being a reciprocal lattice vector. These elements form a subgroup of D_{6h}, known as a little cogroup or simply *k*-group at **k**,[35] which determines the possible symmetries of the electronic states at **k**. At the high-symmetry point *K* (or *K*′) of graphene's Brillouin zone, the *k*-group is D_{3h}, and Bloch functions built as linear combinations of p_z orbitals span a two-dimensional irreducible representation (irrep) of such a symmetry group (E''). This is enough for the $\pi-\pi^*$ degeneracy and the unusual linear dispersion at *K* (*K*′). That this occurs exactly at the Fermi level is a consequence of the electron−hole (e−h) symmetry which approximately holds in graphene. Indeed, thanks to this extra symmetry, energy levels are always symmetrically arranged, and at half-filling, the Fermi level lies exactly at the center of the spectrum, where any doubly degenerate level is forced to lay. (Notice that even though e−h symmetry only holds in the nearest-neighbors approximation and in absence of diagonal disorder, the Fermi level always matches the doubly degenerate state at *K* (*K*′) as long as the e−h symmetry breaking does not cause the maximum (minimum) of the valence (conduction) band to exceed the energy at *K*.) In general, the number of doubly degenerate irreps in the BZ determines alone the presence of states (absence of a gap) at the Fermi level. We have recently shown[21] how one can turn such a number to be even at every special point—thus opening a gap in the band structure—by symmetrically removing "p_z orbitals" in forming certain $n \times n$ superlattices. Substitutional defects behave similarly to p_z vacancies (to which they reduce when the hoppings become zero) but introduce impurity bands which partially hybridize with those of the substrate. In addition, the diagonal disorder they introduce breaks e−h symmetry giving rise to a Fermi level shift, i.e., to *p*- and *n*-doping for group IIIA and VA elements, respectively, as recently shown for both graphene[36] and nanotubes.[37] In the weakly defective superstructures considered in the following, the defect-induced perturbation affects the electronic structure close to the Fermi level. With homogeneous doping the latter shifts at most proportionally to $1/n$, i.e., as the square root of the defect concentration, as a consequence of the linear-energy dispersion which implies $E_F = v_F(\pi n_e)^{1/2}$, where v_F is the Fermi velocity of pristine graphene and n_e is the electron (hole) excess density, $n_e \propto 1/n^2$. Hence, analogously to the superlattices of p_z vacancies,[21] we make use of symmetry arguments to establish whether degeneracy occurs at the BZ special points in the important low-energy region. It is worth noticing at this point that, however small the defect

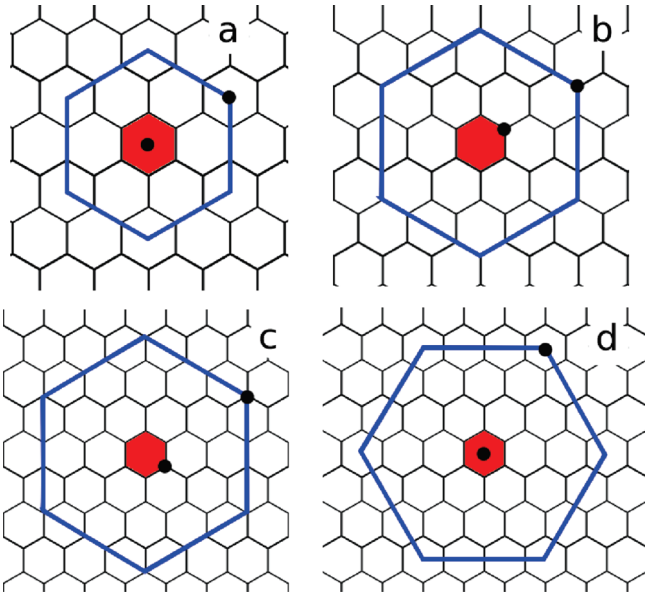

Figure 1. Folding of graphene Brillouin zone (BZ, blue line) into the superlattice ones (red filled hexagon) for some $n \times n$ structures, (a) $n = 3m$, (b) $n = 3m + 1$, and (c) $n = 3m + 2$, along with the case of $\sqrt{3n} \times \sqrt{3n}R30°$ superlattices (d). The K point in graphene's BZ is labeled with a black filled dot.

perturbation is, the folding of graphene band structure occurs differently according to whether the superlattice constant n belongs to the sequence $n = 3m$ or $n = 3m + 1$, $3m + 2$ (m integer). As shown in Figure 1 for the superlattices considered in this work (a−c), for $n = 3m + 1$ ($3m + 2$), K and K' fold separately into $K_n(K'_n)$ and $K'_n(K_n)$, whereas for $n = 3m$ they both fold to the BZ center Γ_n. This means that $n = 3m$ superlattices are expected to have rather unique properties related to the highly degenerate nature of the unperturbed spectrum. In the following, we mainly focus on $n = 3m + 1$, $3m + 2$ superlattices and only occasionally look at the properties of $n = 3m$ ones. A further six-fold superlattice symmetry, the $\sqrt{3n} \times \sqrt{3n}R30°$ case reported in Figure 1(d), will not be considered here since in that case band folding occurs analogously to the $3m \times 3m$ case discussed above.

Honeycomb Superlattices. A honeycomb-shaped superlattice is a natural choice for $n \times n$ superlattices ($n \times n$ honeycombs thereafter) since it preserves the D_{6h} point group symmetry of pristine graphene. The superlattice unit cell contains two substitutional atoms and is shown in Figure 2. If the atomic radii of the dopants are small enough that lattice distortions are minimal, the system overall symmetry is preserved, and Dirac cones at K_n and K'_n are expected. This is the case for boron and nitrogen substitutional defects, whose DFT-optimized structures show no appreciable lattice distortion. Both TB and DFT calculations confirm that $n = 3m + 1$ and $3m + 2$ honeycomb superlattices made of B or N substitutional defects only show a low-energy band structure very similar to that of perfect graphene but with the Fermi level lying, respectively, below (p-doped) and above (n-doped) their Dirac point. In principle, with properly designed n- or p-back-doping, e.g., electric-field induced but also via molecular adsorption,[38,39] such a shift can be offset and the analogy with pristine graphene fully exploited.

Figure 3(a) shows the TB and *first-principles* band structures of one $n \times n$ honeycomb together with the position of the Fermi level (Figure 3(c)) in such n- and p-doped superlattices at

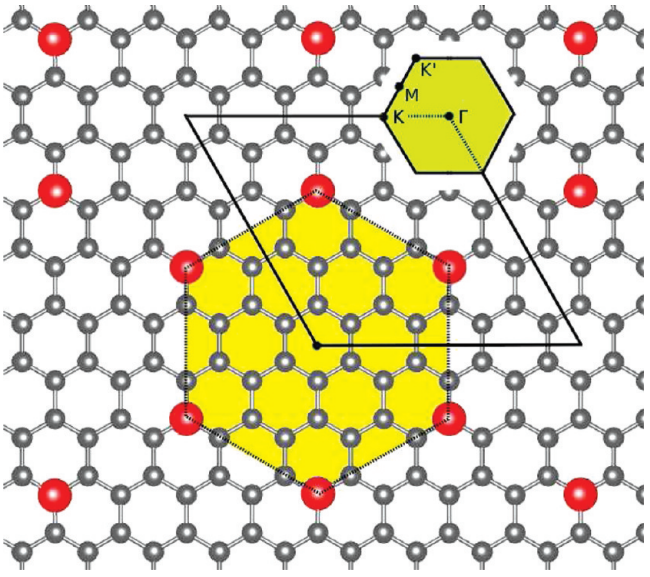

Figure 2. 4×4 Honeycomb superlattice: the black line represents the unit cell, while the Wigner−Seitz and Brillouin zones are shown in yellow and green, respectively. Red balls are sublattice substitutional defects forming the superlattice.

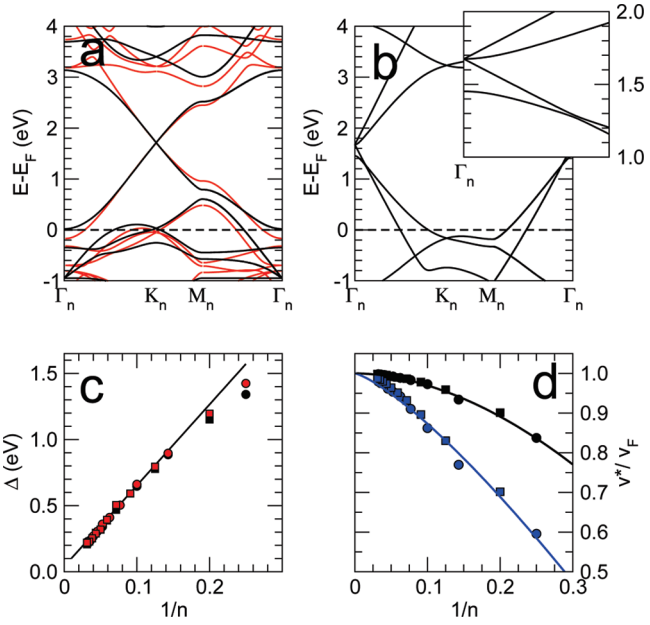

Figure 3. (a) TB (black lines) and DFT (red lines) band structures for the 4×4 honeycomb boron superlattice. (b) the TB band structure of the 3×3 honeycomb boron superlattice arising from folding in $n = 3m$ superlattices. The inset shows a close-up of the region close to Γ_n. (c) Absolute shift of the Dirac cones apex (Δ) with respect to the Fermi level, in p-doped (B, red) and n-doped (N, black) honeycombs. (d) Group velocity for charge carriers close to the cone apex for the boron (black) and nitrogen (blue) case. Circles and squares for $n = 3m + 1$ and $n = 3m + 2$.

different impurity concentrations. As expected, the shift (Δ) of the Dirac cones with respect to the Fermi level (see Figure 3(c)) is, to a good approximation, inversely proportional to the dopant concentration for both B and N doping, though with opposite sign. The difference between TB and DFT band structure is

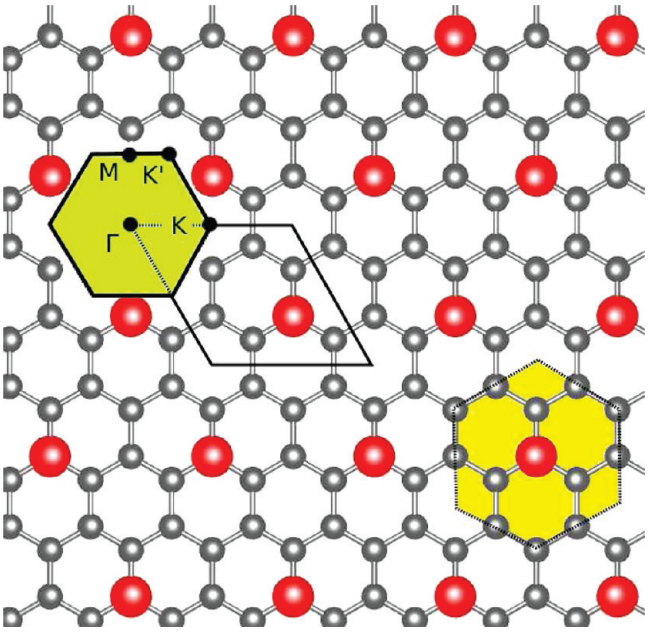

Figure 4. 2 × 2 Hexagon superlattice: the black line represents the unit cell boundary, while the Wigner−Seitz and Brillouin zones are filled in yellow and green, respectively. Red balls are substitutional defect positions.

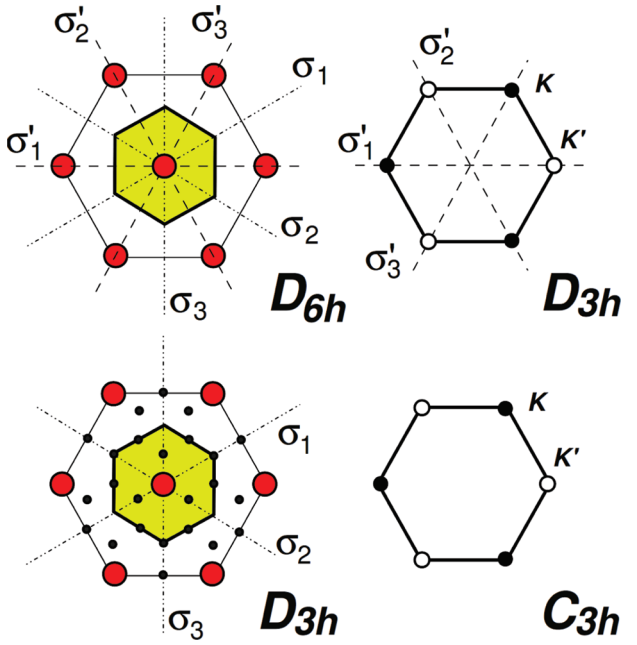

Figure 5. Wigner−Seitz (yellow, left side) and Brillouin zone (right side) for the hexagonal superlattices. Considering the defects only, the point group is D_{6h}, and the corresponding k-group in K_n is D_{3h} (upper panel). Overall, the underlying carbons remove the σ' planes, reducing the symmetry to D_{3h}.

minimal, and this confirms that the tight binding parameters adopted are good enough for accurately describing the low-energy features of the $n \times n$ honeycomb superlattices investigated in this paper. In Figure 3(b) we also report the unique band structure resulting from the special folding in the $n = 3m$ sequence; as it is evident from the inset of Figure 3(b), the 4-fold degeneracy occurring at Γ_n is partially lifted, and a gap is introduced in one of the two cone replica.

The group velocity for electrons and holes taken close to the cone apex (but rather adequate for a wider energy range) is shown in Figure 3(d) for n- and p-doped superlattices. The two curves approach the limit of clean graphene with different trends. Upon nonlinear curve fitting, the group velocity v (relative to the one in pristine graphene) for p-doped honeycombs is found to behave as $v/v_F \propto 1 - n^{-1.29}$ and for n-doped honeycombs as $\propto 1 - n^{-1.84}$. The difference between the two cases is due to the value of the on-site energies and hopping of the dopants which determine the degree of hybridization of their impurity levels with that of bulk graphene. With the parameters used (see Table 1), which are symmetric with respect to the on-site energy of C atoms, this can only happen because of the asymmetry in graphene electronic structure introduced by the next-to-nearest neighbor interactions.

Other superlattices made of group IIIA (Al, Ga, In) and VA (P, As, Sb) dopants have been tested by *first-principles* calculations. In any case, we found that, after geometric optimization of the lattice structure, the impurities stand out from the graphene layer plane and considerably distort the neighboring lattice positions. The resulting band structures are metallic but lack Dirac cones due to the reduced symmetry.

Hexagonal Superlattices. When one defect per supercell only is introduced, a $n \times n$ hexagonal superlattice (a "$n \times n$ hexagon") results, as shown in Figure 4. This kind of structure is closely related to the honeycomb ones, having one extra substitutional atom at the center of a hexagon of defects. A closer inspection, however, reveals that, due to the presence of the underlying C network, the point symmetry is reduced to D_{3h}, with σ' planes missing with respect to the honeycomb counterparts. It follows that the k-group at K_n (K'_n) is C_{3h}, with no irreducible two-dimensional (complex) representations (see Figure 5). Hence, degeneracy is removed at the special points, and a (small) gap opens in the band structures, close to the (shifted) Fermi energy. This is shown in Figure 6(a) where the TB and DFT band structures of the 4 × 4 hexagon are reported. The energy spectrum of such gapped graphene is compatible with charge carriers behaving as *massive* Dirac particles

$$E(\mathbf{k}) = \pm v\sqrt{k_x^2 + k_y^2 + m^{*2}v^2} \qquad (1)$$

where v, and m* are the effective "speed of light" and "rest mass", respectively, and determine the gap size

$$\Delta E = 2m^*v^2 \qquad (2)$$

According to the semiclassical theory of conduction, m^* is also the effective mass m_{eff} governing charge carrier mobility for $k \ll mv$; for $k \gg mv$, carriers behave pseudorelativistically with $m_{eff} = 0$ and limiting speed v. The values v, m^*, and ΔE have been obtained by nonlinear curve fitting of the numerical results to eq 1 and are reported in panels (b)−(d) of Figure 6. For $n \times n$ hexagons the band gap is very dependent on the type of dopant (Figure 6(e)): the maximum gaps, occurring in 2 × 2 hexagons, are 0.93 eV for nitrogen and only 0.17 eV for boron. The effective masses of electrons and holes (Figure 6(d)) roughly scale as the gaps $\propto n^{-1.45}$ and $\propto n^{-1.52}$ for n- and p-doped structures, respectively, and their maximum is 3.7×10^{-2} and 6.7×10^{-3} m_e. This is similar to the case of a graphene nanoribbon,[40] whose band gap scales as the inverse of their width even though here the gap is due to symmetry breaking rather than quantum confinement.

dx.doi.org/10.1021/jp109741s |J. Phys. Chem. C 2011, 115, 3250–3256

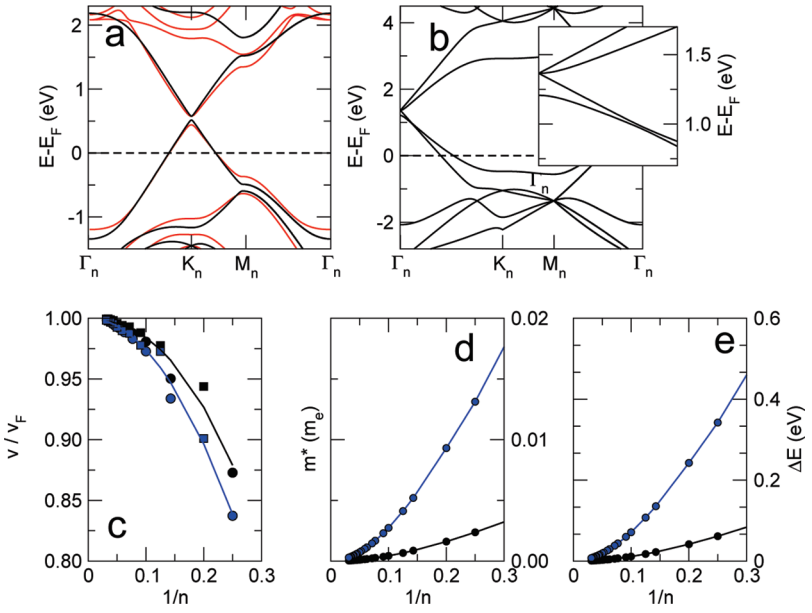

Figure 6. (a) TB (black) and DFT (red) band structures for the 4 × 4 hexagon of boron dopants. (b) The TB band structure of the 3 × 3 hexagon superlattice arising from folding in $n = 3m$ superlattices. The inset shows a close-up of the region close to Γ_n. Carriers effective speeds (c), masses (d), and energy band-gaps (e) versus $1/n$. Black and blue values refer to B and N superlattices, respectively.

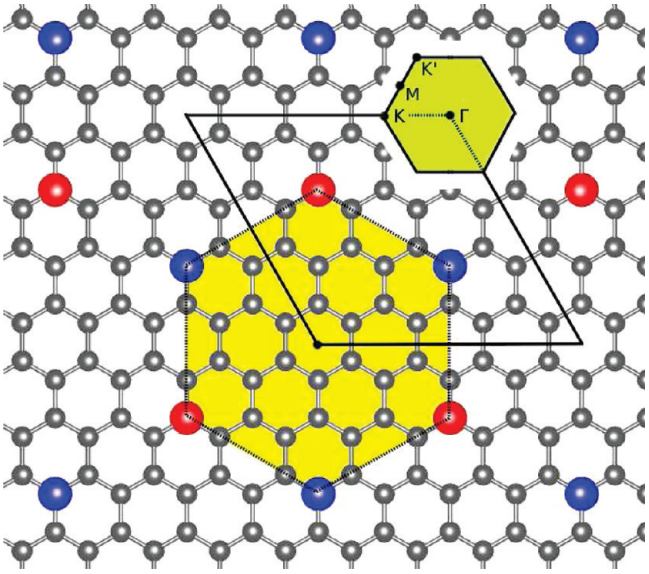

Figure 7. 4 × 4 Honeycomb superlattice: the black line represents the unit cell, while the Wigner−Seitz and Brillouin zone are shown in yellow and green, respectively. Red and blue balls are B and N substitutional defects.

The shift of the Fermi level (not shown) is again proportional to the square root of the defect concentration, that is now only half of the value for honeycombs with the same superlattice periodicity. Charge carrier velocities scale similarly for the two dopant species as shown in Figure 6(c) with a best-fit exponent close to −2 ($v(B)/v_F \propto 1 - n^{-1.98}$, $v(N)/v_F \propto 1 - n^{-2.28}$).

In Figure 6, panel (b), we also report the particular band structure arising in $n = 3m$ hexagon superlattices. At the relevant special point Γ_n, the massive, pseudorelativistic energy dispersion is superimposed with a massless one, thereby giving rise to a two-valley system with very different charge carriers. As shown in the next subsection, all the features discussed in this section can be brought at the Fermi level by codoping the substrate in forming a honeycomb structure with the same D_{3h} symmetry discussed here.

Codoped Superlattices. One further possible superlattice arrangement is obtained by using two different dopants in the $n \times n$ honeycomb unit cell, i.e., codoping the structures with boron and nitrogen (see Figure 7). In this way, B and N atoms form a boron nitride-like honeycomb superlattice in which sublattice equivalence (and symmetry) is broken. This is analogous to placing graphene in the modulating field of a proper substrate, e.g., a hexagonal BN (0001) surface, which has been shown to lift the degeneracy of the $\pi-\pi^*$ bands,[41] similarly for deposition, or growth, on silicon carbide surfaces.[42,43] The superlattice structures considered here offer the possibility to modify the periodicity of the perturbation and thus to tune the gap. Indeed, this kind of superlattice presents D_{3h} point symmetry and hence a C_{3h} k-group in K_n, K'_n and, analogously to the hexagonal case discussed above, opens a band gap typical of massive Dirac particles. Differently from before, however, the structures considered here are iso-electronic with graphene, and therefore the gap lies exactly at the Fermi energy.

Figure 8 shows the computed band structure (panel (a)), together with the values of the effective speed of light (c), effective mass (d), and band gaps (e), obtained as in a previous section by fitting of the numerical results, for different BN $n \times n$ honeycombs. The results confirm the expectations and show that such structures present a band gap at the Fermi energy, compatible with pseudorelativistic massive carriers. Their effective rest mass is rather small, scales as $\propto n^{-1.46}$, and is never larger than 0.015 m_e for $n \geq 4$. This value compares favorably with the effective masses in $Bi_{1-x}Sb_x$ topological insulators ($m^* = 0.009m_e$)[44] and is generally lower than in bilayer graphene ($m^* = 0.03\ m_e$)[45] or in any other traditional bulk semiconductors, such as InSb ($m^* = 0.016m_e$). Since m^* is the main factor affecting carrier mobilities, the suggested structures turn out to be a good compromise

dx.doi.org/10.1021/jp109741s |J. Phys. Chem. C 2011, 115, 3250–3256

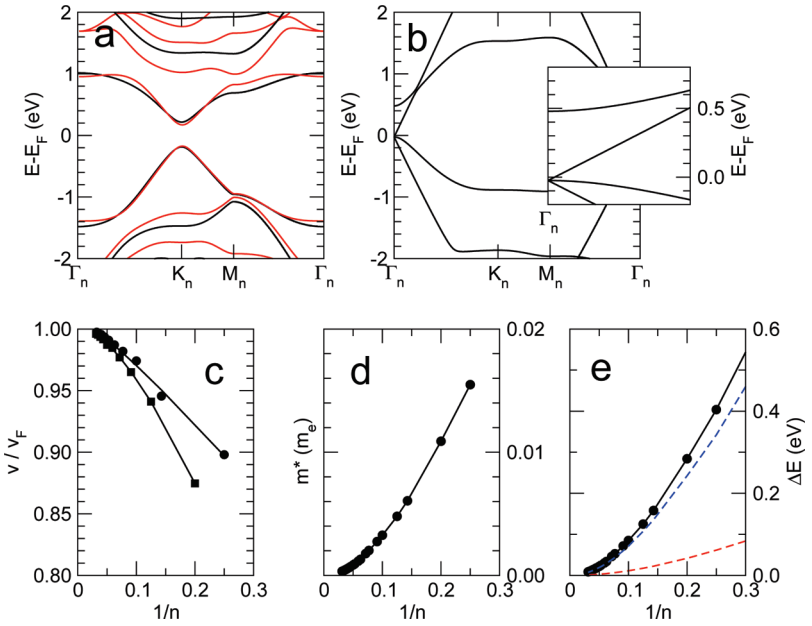

Figure 8. (a) TB (black) and DFT (red) band structures for the codoped 4 × 4 honeycomb. (b) The case of 3 × 3 superlattice with the low-energy region in the inset. (c) Effective speed. (d) Mass at the K_n point versus $1/n$. (e) Band gap. The red and blue dashed lines are the values for n- and p-doped hexagons, shown for comparison.

between the need of opening a gap for logic applications and the desire of preserving the high mobility of charge carriers. In Figure 8, panel (b), we also report the band structure of the $n = 3m$ case. The structure is that of a zero-gap semiconductor, with two distinct charge carriers: one of them behaves as an electron (hole) in graphene, showing typical effects expected for massless carriers, and the other is a more conventional one, with a finite excitation energy across a gap.

SUMMARY AND CONCLUSIONS

To summarize, we have studied the effects substitutional defects such B and N species have on graphene electronic structure when they are periodically arranged to form some superlattices. Using group theoretical arguments and both TB and DFT calculations, we have shown that defects can either preserve the Dirac cones or open a band gap, depending on the superlattice symmetry (D_{6h} and D_{3h}, respectively). Specifically, honeycomb-shaped superlattices of B or N atoms give rise to p- and n-doped graphene, respectively, preserving the Dirac cones. On the other hand, when a hexagonal superlattice is formed, or the honeycomb one is symmetrically codoped, the Dirac cones detach from each other to form a gapped, quasi-conical structure whose excitations correspond to massive Dirac particles. Note that this situation clearly differs form the case of randomly arranged B or N impurities, in which the density of states shows no band gap.[36]

For zero-gap structures, the use of these superlattices offers the possibility to control the Fermi velocity by changing the structure periodicity, thereby offering the opportunity to investigate its role in the charge transport properties. Differently from our recent proposal,[21] the gapped band structures arise because of symmetry breaking, as in the case of graphene interacting with a substrate such as SiC or BN. In the same fashion, the band gap size depends on the superlattice periodicity. In our calculations, we have found that band gaps, charge carrier velocities and effective masses depend on $1/n^p$, where p is in the range 1−2, hence on some small power (0.5−1) of the dopant concentration, and on the dopant type (B or N). Overall the structures proposed here show a band gap larger than k_BT at room temperature, with an effective mass generally lower than $0.01m_e$ for reasonably dense meshes ($n = 4-10$). Thus, the new class of graphene structures proposed might be promising candidates for the fabrication of high-performance interconnects and valley-based devices,[46] but also for logic transistors, where a band gap is needed, but the extraordinary properties of pristine graphene need to be preserved.

The electronic properties of these superlattices of impurities rely on symmetry and hence are necessarily sensitive to the dopant positions. As a consequence, an accurate control of the system geometry is necessary to exploit their properties. This might be possible in the near future with precise bottom-up synthesis techniques, such as the ones recently used by Bieri et al. and Cai et al.[19,20] to fabricate nanoribbons with well-defined widths and edges.

ASSOCIATED CONTENT

Supporting Information. An indication of the possible synthetic routes together with formation energies for such superlattices of defects can be found. This material is available free of charge via the Internet at http://pubs.acs.org.

AUTHOR INFORMATION

Corresponding Author

*E-mail: simone.casolo@unimi.it; rocco.martinazzo@unimi.it.

REFERENCES

(1) Slonczewski, J. C.; Weiss, P. R. *Phys. Rev.* **1958**, *109*, 272.
(2) Castro Neto, A. H.; Guinea, F.; Peres, N. M. R.; Novoselov, K. S.; Geim, A. K. *Rev. Mod. Phys.* **2009**, *81*, 109.
(3) Abergel, D. S. L.; Apalkov, V.; Berashevich, J.; Ziegler, K.; Chakraborty, T. *Adv. Phys.* **2010**, *59*, 261.
(4) Schwierz, F. *Nature Nanotech.* **2010**, *5*, 487.

(5) Lin, Y.-M.; Jenkins, K. A.; A. Valdes-Garcia, J. P. S.; Farmer, D. B.; Avouris, P. *Nano Lett.* **2009**, *9*, 422.
(6) Avouris, P. *Nano Lett.* **2010**, *10*, 4285.
(7) Peres, N. M. R. *Rev. Mod. Phys.* **2010**, *82*, 2673.
(8) Avouris, P.; Chen, Z.; Perebeinos, V. *Nat. Nanotech.* **2007**, *2*, 605.
(9) Tiwari, R. P.; Stroud, D. *Phys. Rev. B* **2009**, *79*, 205435.
(10) Park, C.; Yang, L.; Son, Y.; Cohen, M. L.; Louie, S. G. *Phys. Rev. Lett.* **2008**, *101*, 126804.
(11) Pedersen, T. G.; Flindt, C.; Pedersen, J.; Mortensen, N. A.; Jauho, A.; Pedersen, K. *Phys. Rev. Lett.* **2008**, *100*, 136804.
(12) Liu, W.; Zhang, Z. F.; Shi, Q. W.; Yang, J.; Liu, F. *Phys. Rev. B* **2009**, *80*, 233405.
(13) Chernozatonskii, L. A.; Sorokin, P. B. *J. Phys. Chem. C* **2010**, *114*, 3225.
(14) Fischbein, M.; Drni'c, M. *Appl. Phys. Lett.* **2008**, *93*, 113107.
(15) Bai, J. W.; Zhong, X.; Jiang, S.; Y, Y. H.; Duan, X. F. *Nature Nanotechnol.* **2010**, *5*, 190.
(16) Balog, R.; et al. *Nat. Mater.* **2010**, *4*, 315.
(17) Cheianov, V. V.; Syljuåsen, O.; Altshuler, B. L.; Fal'ko, V. *Phys. Rev. B* **2009**, *80*, 233409.
(18) Cheianov, V. V.; Syljuåsen, O.; Altshuler, B. L.; Fal'ko, V. *Europhys. Lett.* **2010**, *89*, 56003.
(19) Bieri, M.; Treier, M.; Cai, J.; Aït-Mansour, K.; Ruffieux, P.; Gröning, O.; Gröning, P.; Kastler, M.; Rieger, R.; Feng, X.; Müllen, K.; Fasel, R. *Chem. Commun.* **2009**, *45*, 470.
(20) Cai, J.; Ruffieux, P.; Jaafar, R.; Bieri, M.; Braun, T.; Blankenburg, S.; Muoth, M.; Seitsonen, A.; Saleh, M.; Feng, X.; Müllen, K.; Fasel, R. *Nature* **2010**, *466*, 470.
(21) Martinazzo, R.; Casolo, S.; Tantardini, G. F. *Phys. Rev. B* **2010**, *81*, 245420.
(22) Dutta, S.; Manna, A. K.; Pati, S. K. *Phys. Rev. Lett.* **2009**, *102*, 0966011.
(23) Dutta, S.; Pati, S. K. *J. Phys. Chem. B* **2008**, *112*, 1333.
(24) Zheng, X. H.; Wang, X. L.; Abtew, T. A.; Zeng, Z. *J. Phys. Chem. C* **2010**, *114*, 4190.
(25) Yu, S. S.; Zheng, W. T. *Nanoscale* **2010**, *2*, 1069.
(26) Dutta, S.; Pati, S. K. *J. Mater. Chem.* **2010**, *20*, 8207.
(27) Panchakarla, L. S.; Subrahmanyam, K. S.; Saha, S.; Govindaraj, A.; Krishnamurthy, H. R.; Waghmare, U. V.; Rao, C. N. R. *Adv. Mater.* **2009**, *21*, 4726.
(28) Ci, L.; Song, L.; Jin, C.; Jariwala, D.; Wu, D.; Li, Y.; Srivastava, A.; Wang, Z. F.; Storr, K.; Balicas, L.; Liu, F.; Ajayan, P. M. *Nat. Mater.* **2010**, *9*, 430.
(29) Pontes, R. B.; Fazzio, A.; Dalpian, G. M. *Phys. Rev. B* **2009**, *79*, 033412.
(30) Nanda, B. R. K.; Satpathy, S. *Phys. Rev. B* **2009**, *80*, 165430.
(31) Peres, N. M. R.; Klironomos, F. D.; Tsai, S. W.; Santos, J. R.; Lopes dos Santos, J. M. B.; Castro Neto, A. H. *Europhys. Lett.* **2007**, *80*, 67007.
(32) Kresse, G.; Hafner, J. *Phys. Rev. B* **1994**, *49*, 14251.
(33) Kresse, G.; Hafner, J. *Phys. Rev. B* **1993**, *47*, 558.
(34) Perdew, J. P.; Burke, K.; Ernzerhof, M. *Phys. Rev. Lett.* **1996**, *77*, 3865.
(35) Mirman, R. *Point groups, space groups, crystals and molecules*; World Scientific: River Edge, NJ, 1999.
(36) Lherbier, A.; Blase, X.; Niquet, Y.; Triozon, F.; Roche, S. *Phys. Rev. Lett.* **2008**, *101*, 036808.
(37) Zheng, B.; Hermet, P.; Hernard, L. *ACS Nano* **2010**, *4*, 4165.
(38) Coletti, C.; Riedl, C.; Lee, D. S.; Krauss, B.; Patthey, L.; von Klitzing, K.; Smet, J. H.; Starke, U. *Phys. Rev. B* **2010**, *81*, 235401.
(39) Pinto, H.; Jones, R.; Goss, J. P.; Briddon, P. R. *Phys. Status Solidi A* **2010**, *207*, 2131.
(40) Barone, V.; Hod, O.; Scuseria, G. *Nano Lett.* **2006**, *6*, 2748.
(41) Giovannetti, G.; Khomyakov, P. A.; Brocks, G.; Kelly, P. J.; van der Brink, J. *Phys. Rev. B* **2007**, *76*, 073103.
(42) Mattausch, A.; Pankratov, O. *Phys. Rev. Lett.* **2007**, *99*, 076802.
(43) Varchon, F.; Feng, R.; Li, X.; Ngoc Nguyen, B.; Naud, C.; Veullien, J. Y.; Berger, C. *Phys. Rev. Lett.* **2007**, *99*, 126805.
(44) Hsieh, D.; Qian, D.; Wray, L.; Xia, Y.; Hor, Y.; Cava, R.; Hasan, M. *Nature* **2008**, *452*, 970.
(45) Castro, E. V.; Peres, N.; Lopes do Santos, J.; Guinea, F.; Castro Neto, A. H. *J. Phys.: Conf. Ser.* **2008**, *129*, 012002.
(46) Xiao, D.; Yao, W.; Niu, Q. *Phys. Rev. Lett.* **2007**, *99*, 236809.